



Supplement of

Measurement report: Impact of cloud processes on secondary organic aerosols at a forested mountain site in southeastern China

Zijun Zhang et al.

Correspondence to: Weiqi Xu (xuweiqi@mail.iap.ac.cn) and Yele Sun (sunyele@mail.iap.ac.cn)

The copyright of individual parts of the supplement might differ from the article licence.

S1. PMF diagnosis

In this study, organic mass spectra together with several selected inorganic ions (SO^+ , SO_2^+ , SO_3^+ , HSO_3^+ , H_2SO_4^+ , NO^+ , NO_2^+ , NH^+ , NH_2^+ , NH_3^+ , Cl^+ , and HCl^+) were analyzed by the PMF. The number of factors from 1 to 5 with f_{Peak} varying from -1 to 1 were evaluated, and the diagnostic plots are shown in Figure S2. In the PMF analysis, the Q/Q_{exp} values represent the ratios between the actual sum of the squares of the scaled residuals (quality-of-fit parameter, Q) obtained from the PMF least square fit and the ideal Q (Q_{exp}) obtained if the fit residuals at each point were equal to the noise specified for each data point. Typically, a strong change in Q/Q_{exp} value with the addition of a factor indicates that more of the variability of the data is explained (Patero and Tapper, 1993; Ulbrich et al., 2009). As shown in Figure S4a, The Q/Q_{exp} value started to greatly decrease from one- (1.52) to three-factor solution (1.05). However, the three-factor solution (including one organic associated with sulfate ions factor ($\text{SO}_4\text{-OA}$), one inorganic nitrate factor (NIA), and one oxygenated OA (OOA)) cannot further differentiate OOA with different oxidation degrees. The four-factor solution, with a Q/Q_{exp} value of 1.0065, can separate two OOA factors with different elemental ratios and temporal variations. Continuing to increase the factor number cannot significantly decrease the Q/Q_{exp} . Furthermore, with 4 factors, the reconstructed mass tracked well with the variations of measured mass, and the scaled residuals of all ion fragments were distributed between -4–4 (Figs. S2c and d), suggesting that they were well reproduced by the PMF model. Therefore, we considered the four-factor solution with $f_{\text{Peak}} = 0$ to be the optimum solution for PMF analysis in this study.

Table S1. Summary of the detailed descriptions for the instruments used during the sampling period, including the measured parameters, model, temporal resolution, and sampling time.

Instrument	Species	Model/Company	Time resolution	Sampling time
Q-ACSM	NR-PM ₁ (Org, SO ₄ , NO ₃ , NH ₄ , Chl)	Aerodyne Research Inc.	20 min	11.1–30
HR-ToF-AMS	NR-PM ₁ (Org, SO ₄ , NO ₃ , NH ₄ , Chl)	Aerodyne Research Inc.	1 min	11.15–20; 11.24–28
AE33	BC	Magee Scientific Corp.	1 min	11.1–30
CO analyzer	CO	Picarro G2401	1 min	11.1–30
Gas analyzers	O ₃ , NO _x	Thermo Scientific	1 min	11.1–30
PM analyzer	PM _{2.5} , PM ₁₀	Thermo Scientific	1 min	11.1–30
Data logger	RH, T, WS, WD, P	CR1000, Campbell Scientific Inc.	1 min	11.1–30
Four-cup anemometers	WS, WD	Model O1OC and O2OC, Met One Instruments Inc.	1 min	11.1–30
P Sensor	P	CS106, Vaisala Ltd.	1 min	11.1–30
T/RH probe	T, RH	HC2S3, Campbell Scientific Inc.	1 min	11.1–30
Particle lidar	Depolarization ratio	Science of Light Technologies Co., Ltd	5 min	11.19–20; 11.25–27

Table S2. The detection limits (in ng m^{-3}) of ACSM (20 min average time) and AMS (1 min average time) for different NR-PM₁ chemical species that are determined as 3 times the standard deviation of mass concentrations during a period (16–20 November) with low particle concentration.

Species	ACSM	AMS
Org	1500	97
SO ₄	497	18
NO ₃	166	28
NH ₄	201	37
Chl	130	7.6

Table S3. Summary of mean mass concentrations (in $\mu\text{g m}^{-3}$) and chemical composition of submicron aerosols measured at selected mountain sites in China.

Location	Mt.	Mt. Tai				Mt.	Mt.	Mt.	
	Wuzhi					Yulong	Daban	Waliguan	
Time	3/19/2015	2011				3/22/2015	9/5/2013	7/1/2017	
	4/15/2015	Spr	Sum	Aut	Win	4/14/2015	10/15/2013	7/31/2017	
Org	Mass	4.8	8.6	16.4	5.7	11.6	3.9	4.9	3.5
	Frac.	43.8 %	28.4 %	29.4 %	31.5 %	31.6 %	68 %	43.2 %	38.1 %
SO ₄	Mass	3.4	7.3	20.1	5.7	8.7	0.8	3.2	3.1
	Frac.	30.9 %	24.1 %	36.0 %	31.5 %	23.7 %	14 %	28.2 %	34.5 %
NO ₃	Mass	0.5	8.8	8.3	3.8	9.6	0.2	1.2	0.7
	Frac.	4.7 %	20.9 %	14.9 %	21.0 %	26.2 %	4 %	10.6 %	8.1 %
NH ₄	Mass	1.5	5.6	11.0	2.9	6.8	0.3	1.4	1.4
	Frac.	13.7 %	18.5 %	19.7 %	16.0 %	18.5 %	5 %	12.3 %	15.2 %
Chl	Mass	0.03					0.14	0.1	
	Frac.	0.3 %					1.2 %	1.1 %	
BC	Mass	0.7				0.5	0.51	0.3	
	Frac.	6.6 %				9 %	4.5 %	3.0 %	
NR-PM ₁	10.2	30.3	55.8	18.1	36.7	5.2	10.9	8.8	
PM ₁	10.9					5.7	11.4	9.1	
References	(Zhu et al., 2016)		(Zhang et al., 2014)			(Zheng et al., 2017)	(Du et al., 2015)	(Zhang et al., 2019)	

Table S4. Summary of main PM₁ chemical components, air pollutants, and meteorological parameters (average \pm standard deviation) during different periods.

Species		Entire study	C1	EP5
	PM ₁	4.29 \pm 4.82	1.34 \pm 0.83	9.39 \pm 5.57
<i>PM₁ species</i> ($\mu\text{g m}^{-3}$)	Org	1.84 \pm 1.63	0.74 \pm 0.48	4.22 \pm 2.54
	NO ₃	0.63 \pm 1.48	0.13 \pm 0.20	1.74 \pm 1.51
	SO ₄	0.72 \pm 0.55	0.09 \pm 0.10	1.54 \pm 0.93
	NH ₄	0.64 \pm 0.78	0.12 \pm 0.10	1.01 \pm 0.66
	Chl	0.02 \pm 0.02	0.01 \pm 0.02	0.06 \pm 0.05
	BC	0.44 \pm 0.36	0.25 \pm 0.14	0.82 \pm 0.47
	<i>Air pollutants</i> (<i>ppbv</i>)	O ₃	13.70 \pm 12.42	4.80 \pm 4.73
NO		0.55 \pm 0.95	0.78 \pm 1.62	0.32 \pm 0.09
NO ₂		3.45 \pm 3.33	5.00 \pm 4.88	2.20 \pm 1.03
CO (ppmv)		0.26 \pm 0.12	0.36 \pm 0.09	0.26 \pm 0.07
PM _{2.5} ($\mu\text{g m}^{-3}$)		6.74 \pm 7.11	2.08 \pm 1.67	15.27 \pm 9.03
PM ₁₀ ($\mu\text{g m}^{-3}$)		15.78 \pm 13.23	NA	21.19 \pm 12.83
<i>Meteorological parameters</i>	<i>T</i> ($^{\circ}\text{C}$)	13.03 \pm 6.13	11.58 \pm 1.92	11.93 \pm 1.64
	RH (%)	86.98 \pm 16.60	100 \pm 0	93.90 \pm 8.11
	WS (m s^{-1})	2.42 \pm 1.24	2.17 \pm 1.51	3.24 \pm 1.83
	<i>P</i> (hPa)	894.28 \pm 3.21	894.43 \pm 1.20	893.29 \pm 1.07

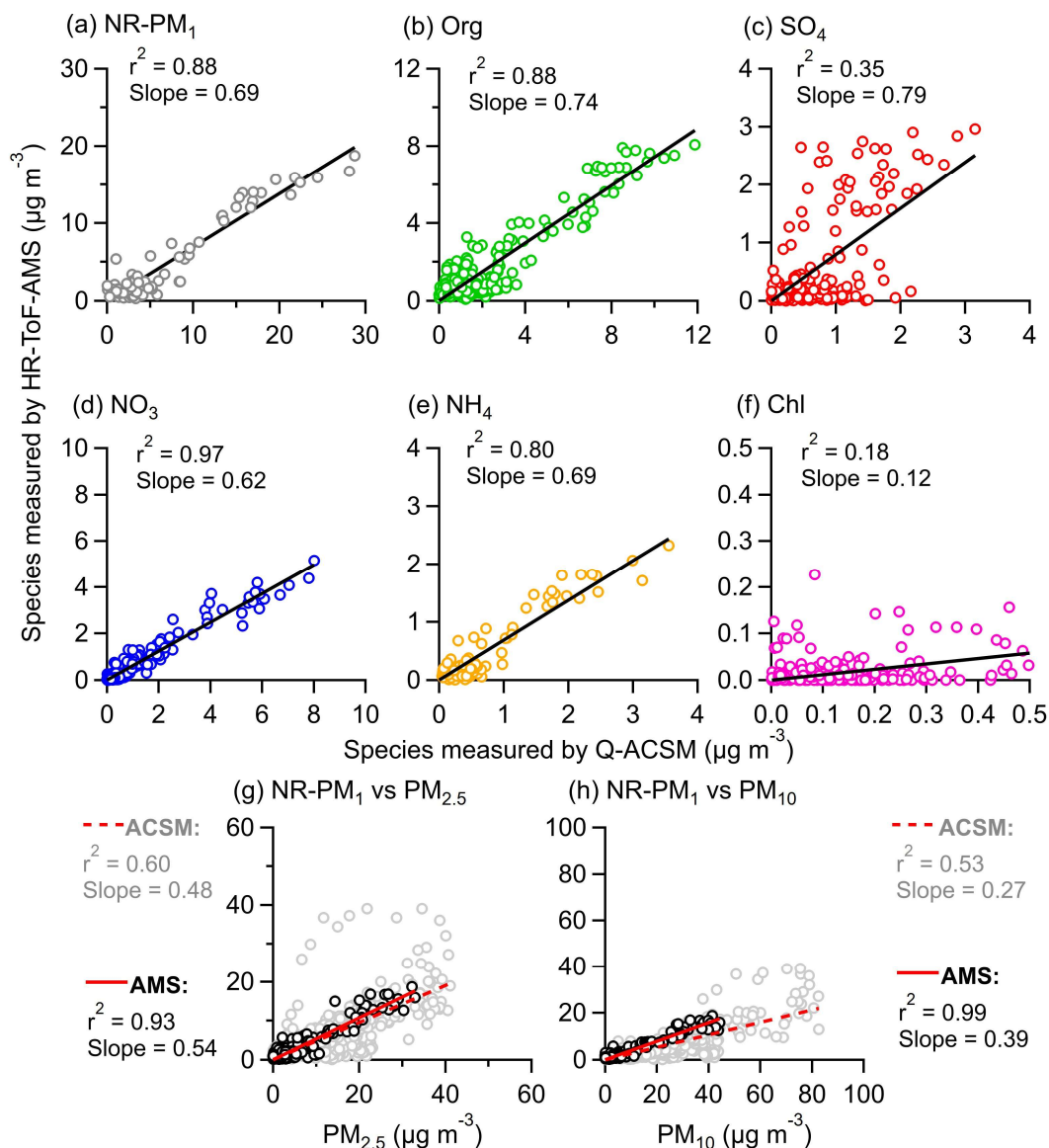


Figure S1. (a-f) Comparison of different NR-PM₁ species measured by ACSM and AMS during the AMS sampling period (15–20, 24–28 Nov); (g-h) Scatter plots of mass concentrations of NR-PM₁ measured by ACSM (grey) and AMS (black) vs. PM_{2.5} and PM₁₀ measured by particulate monitor. The black and red lines are linear-fit lines.

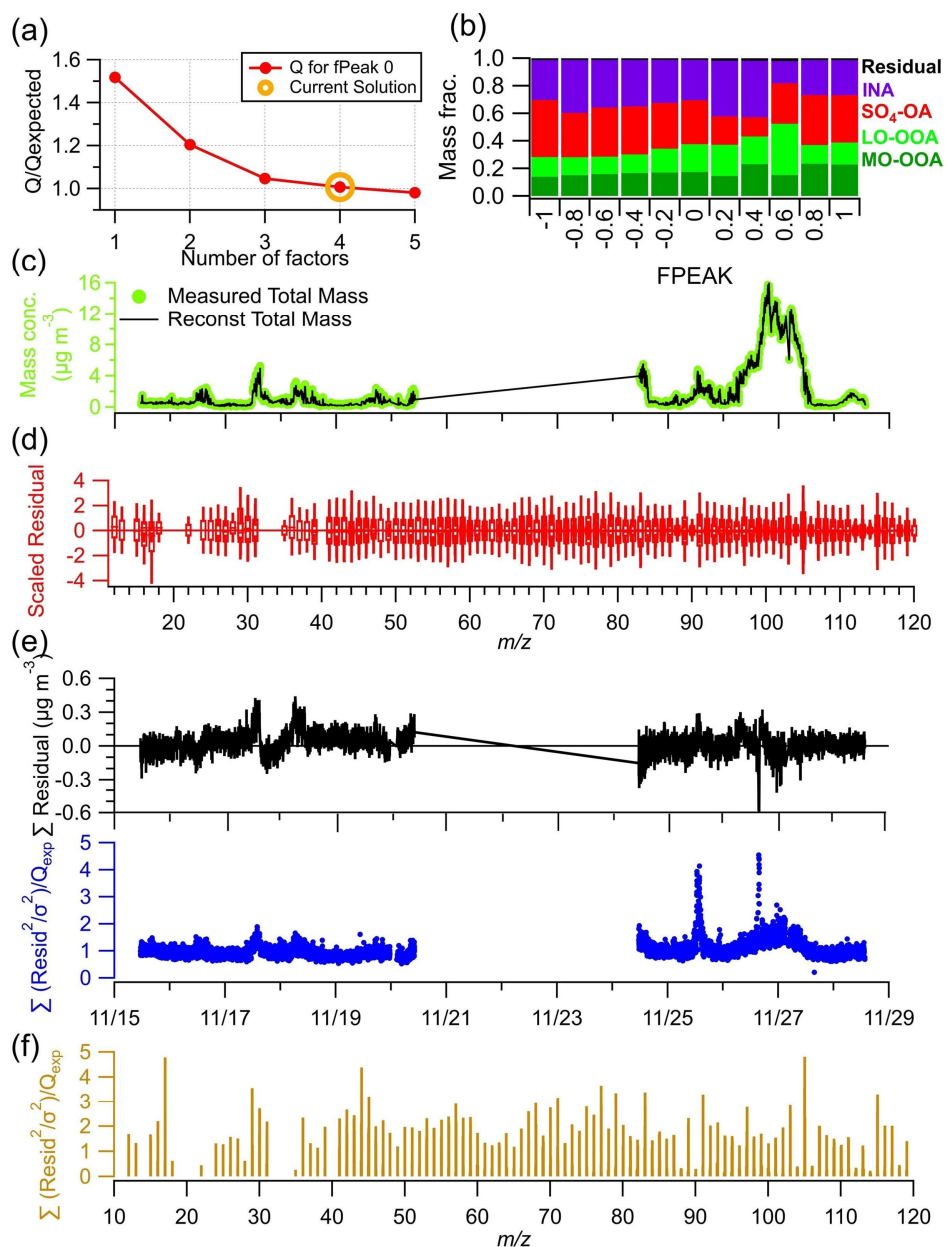


Figure S2. PMF key diagnostic plots: (a) Q/Q_{expected} vs. PMF factors at fPeak = 0; (b) mass fraction of PMF factors vs. fPeak; (c) time series of the reconstructed and measured total organic mass; (d) scaled residual for each mass; (e) time series of the residual of PMF solutions and Q/Q_{expected} ; (f) the Q/Q_{expected} for each mass.

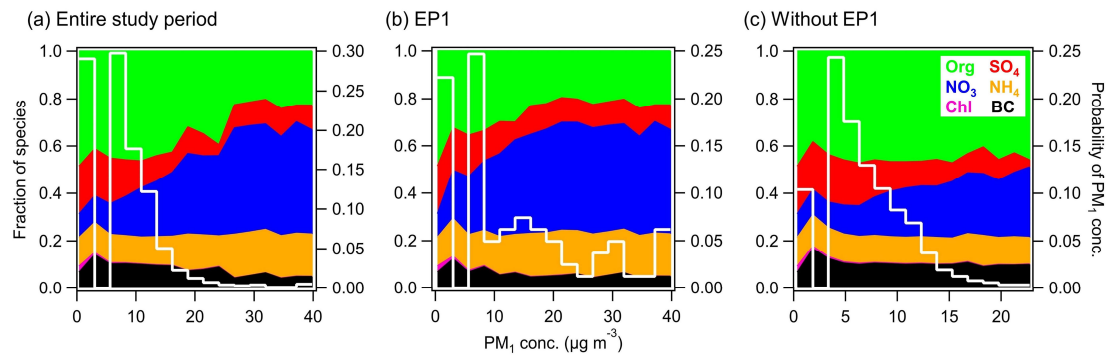


Figure S3. Variations of aerosol composition as a function of PM₁ mass concentration and the probability density of PM₁ during (a) the entire campaign, (b) EP1, and (c) the campaign without EP1.

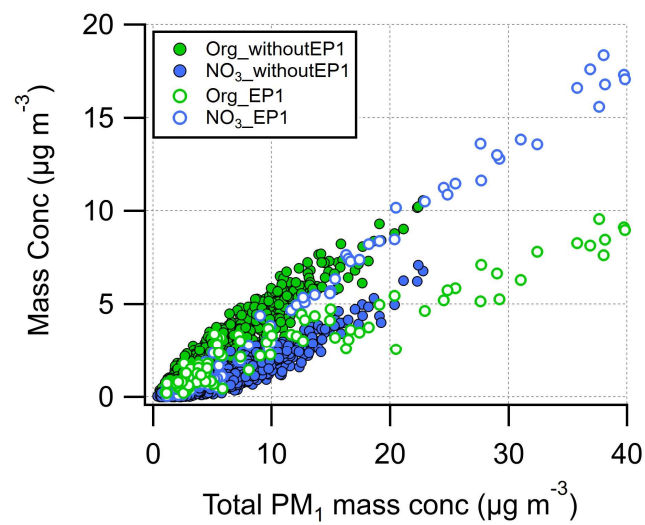


Figure S4. Mass concentrations of organic and nitrate as a function of total PM₁ mass concentration. White circles represent data during the nitrate episode (EP1).

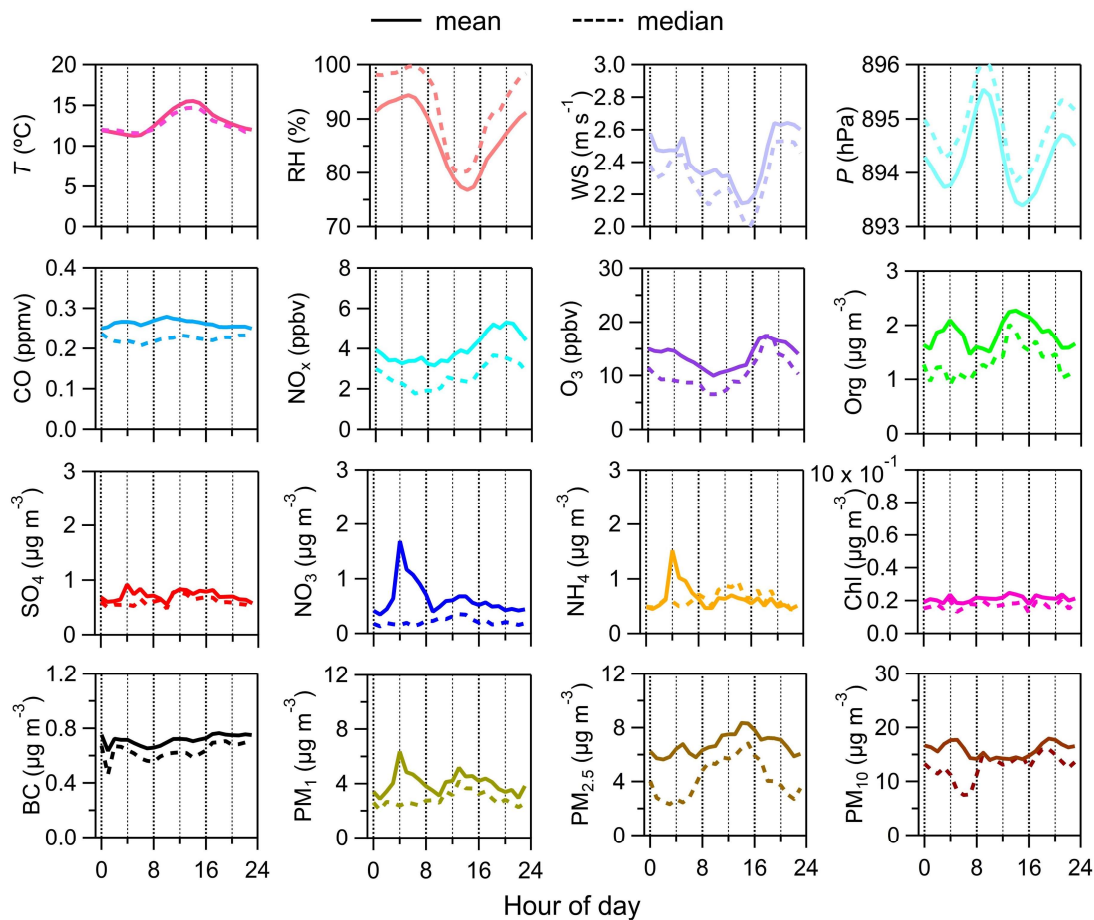


Figure S5. Diurnal variations of PM₁ species (BC + NR-PM₁ measured by ACSM), air pollutants, and meteorological parameters during the entire campaign (1–30 November).

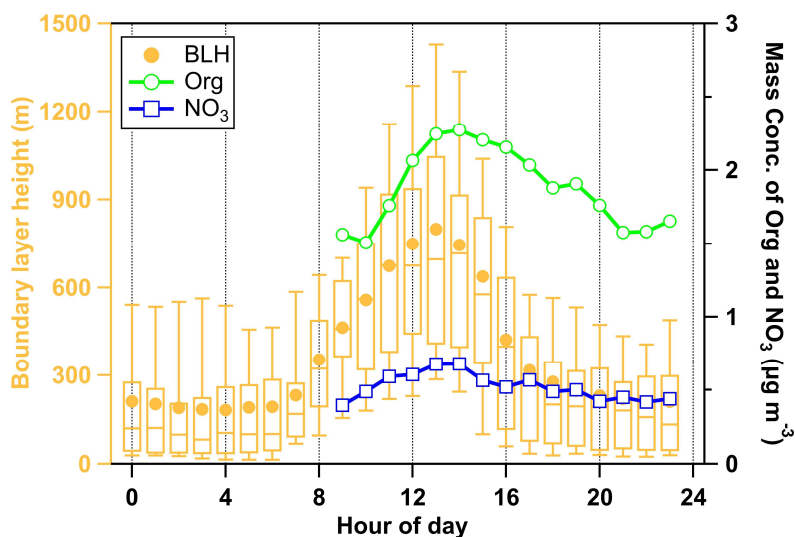


Figure S6. Diurnal variations of boundary layer height along with mass concentrations of organics and nitrate. Data of organics and nitrate before 9:00 was omitted for ease of comparison.

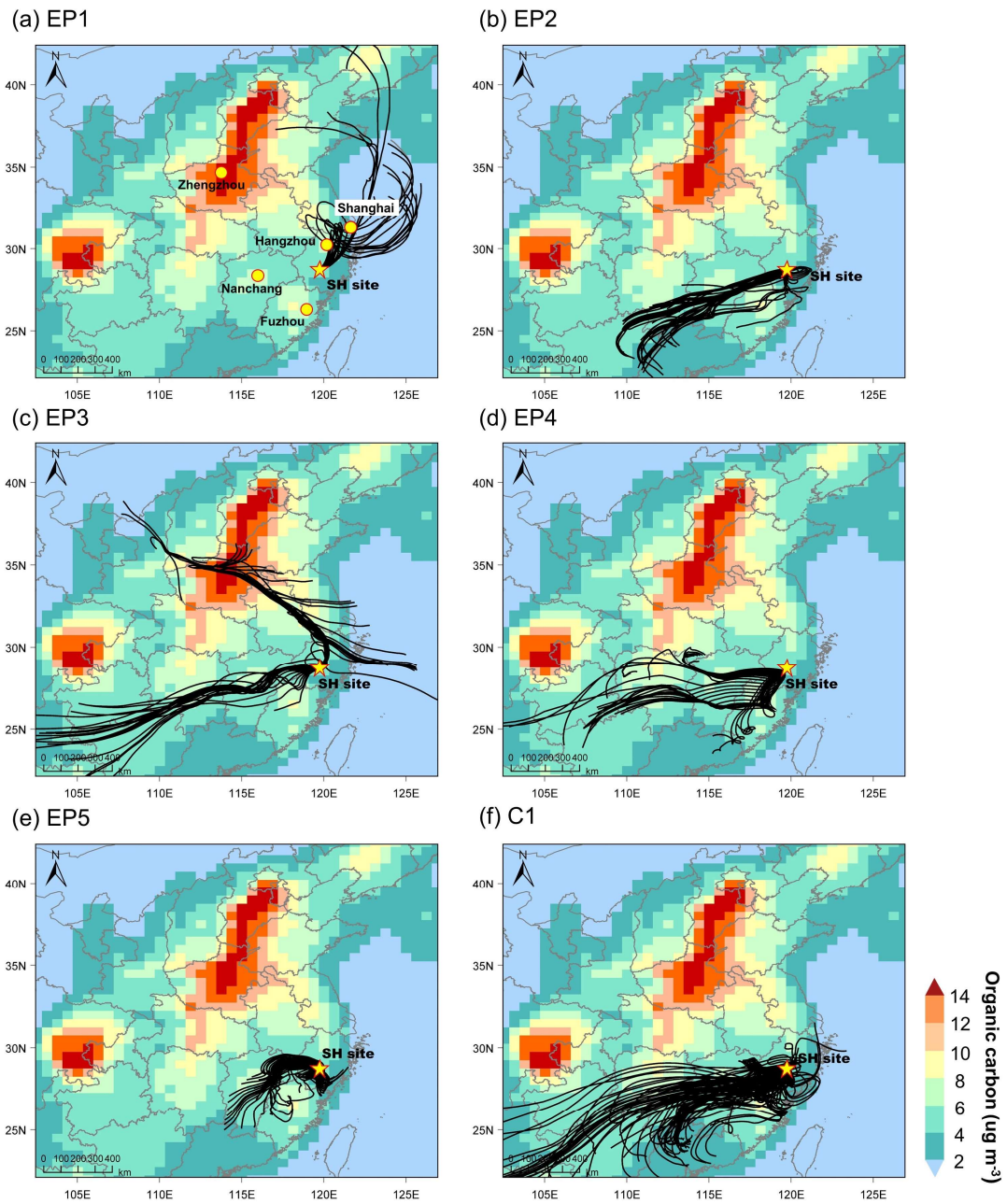


Figure S7. 72 h air mass back trajectories calculated at 1 h intervals at the SH site during six selected periods.

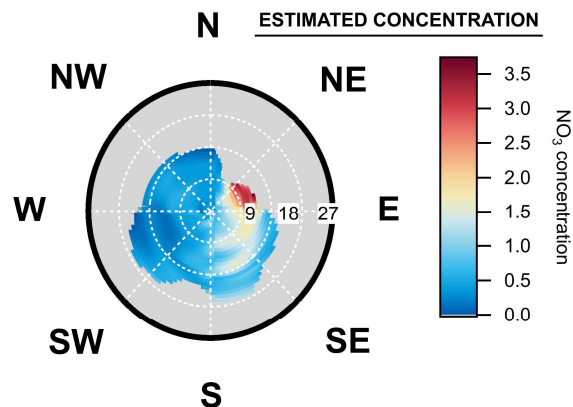


Figure S8. Non-Parametric Wind (NWR) regression polar plot for nitrate calculated for EP1 at the SH site. Analysis was performed using the ZeFir toolbox (Petit et al., 2017) developed within the Igor Pro software.

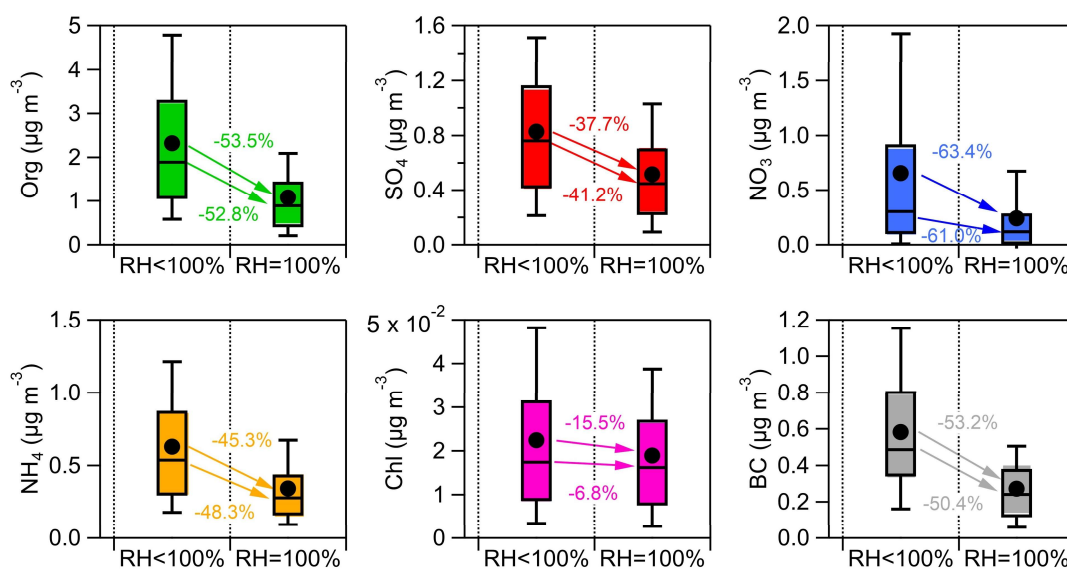


Figure S9. Comparison of mean and median mass concentrations of PM₁ species under conditions of RH below and at 100 % over the campaign without EP1 and EP3.

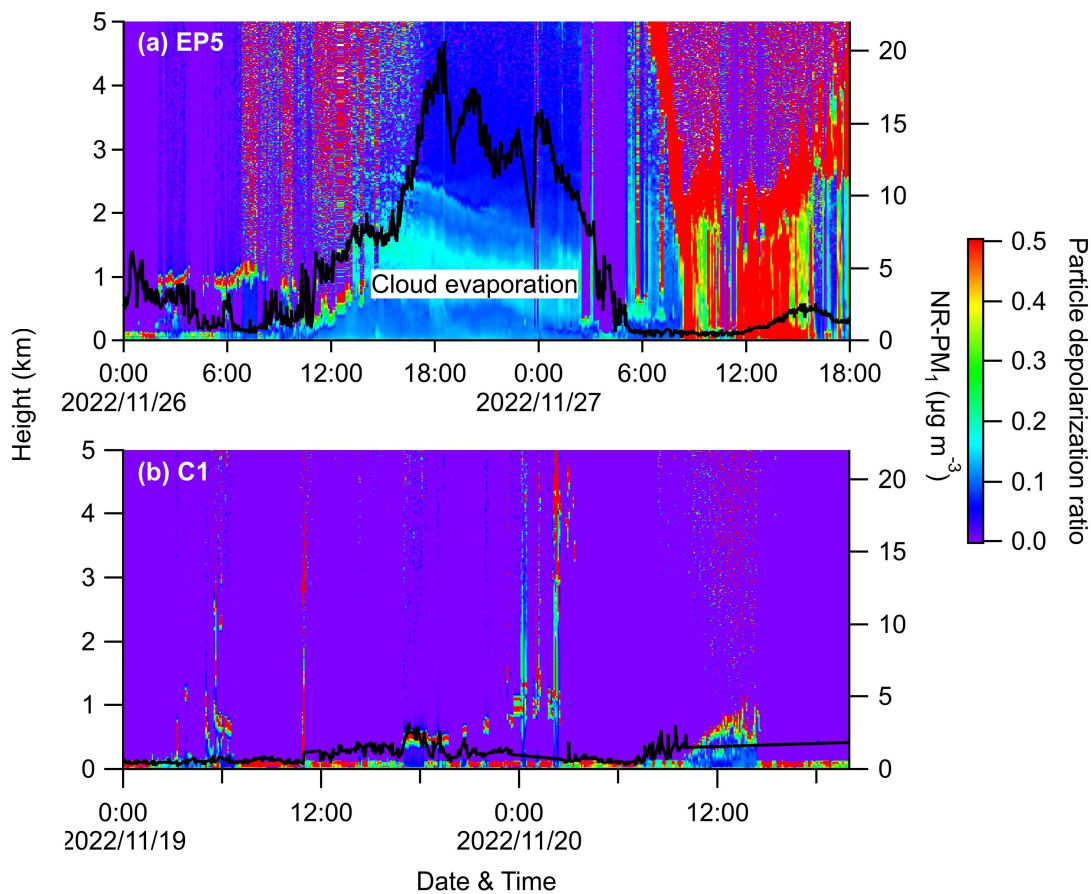


Figure S10. Vertical distribution of particle depolarization ratios in (a) EP5 and (b) C1.

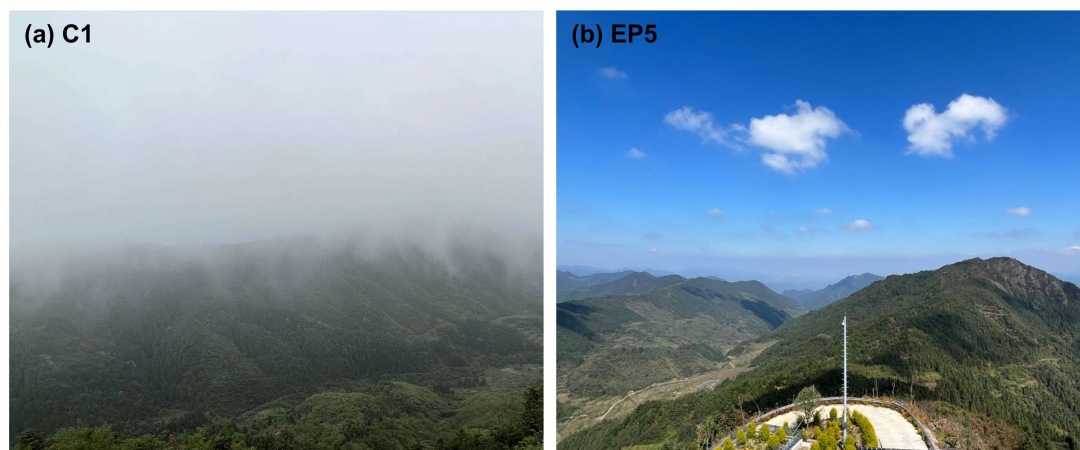


Figure S11. The weather condition in (a) C1 and (b) EP5 (photos were taken on the roof of the sampling site at local time ~15:00 on 19 Nov and 26 Nov).

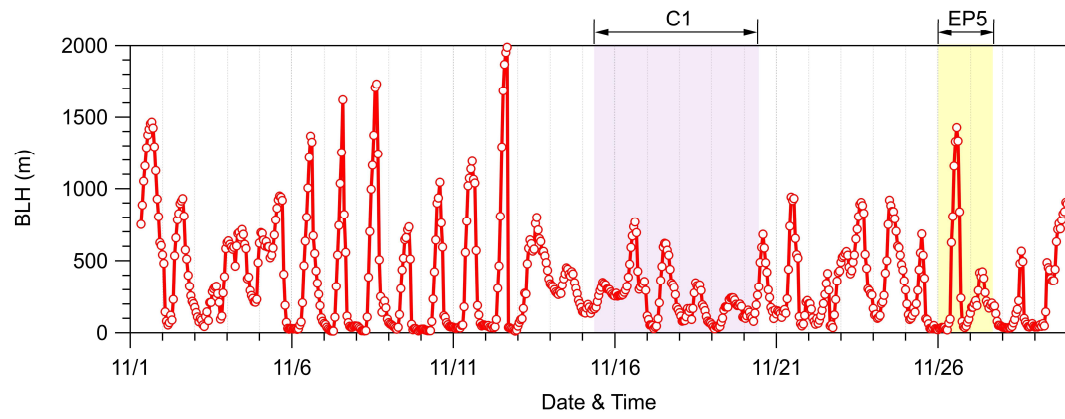


Figure S12. Time series of boundary layer height during the sampling period.

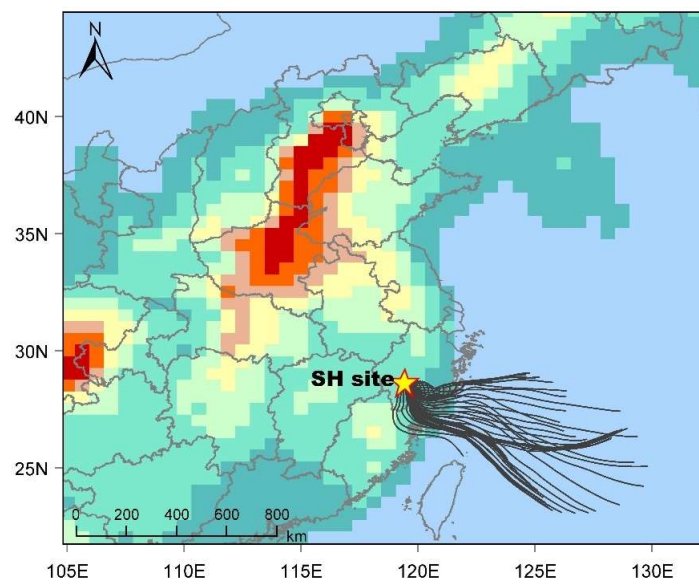


Figure S13. 72 h air mass back trajectories calculated at 1 h intervals at the SH site during 10–12 November.

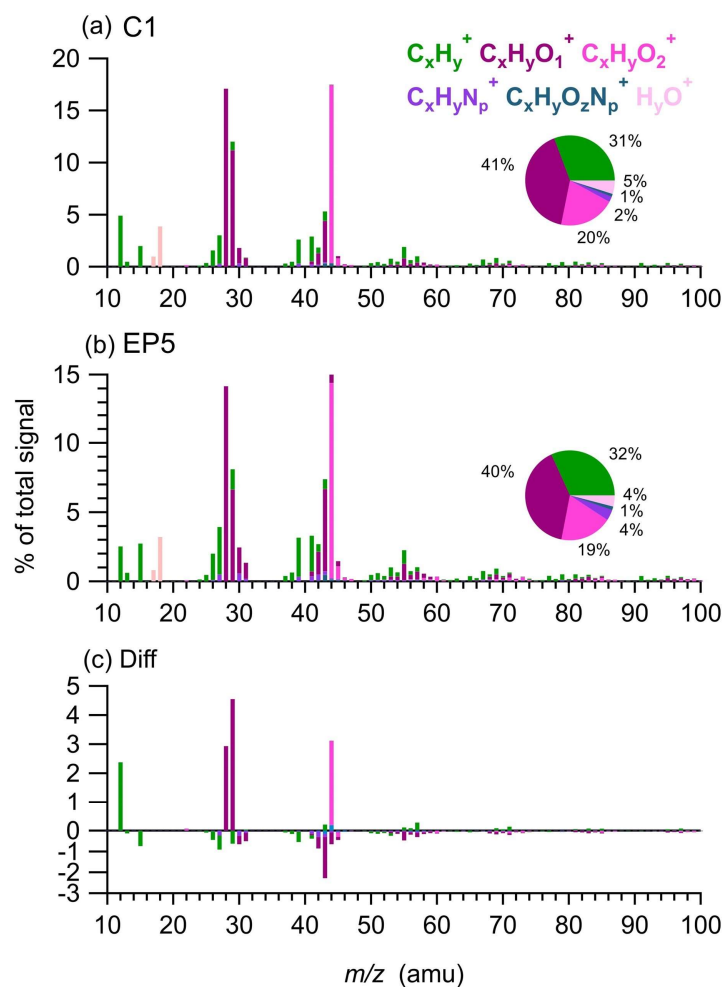


Figure S14. The average high-resolution mass spectra of OA sampled at SH site colored by six ion categories during (a) C1 and (b) EP5, as well as (c) the difference in these two mass spectra.

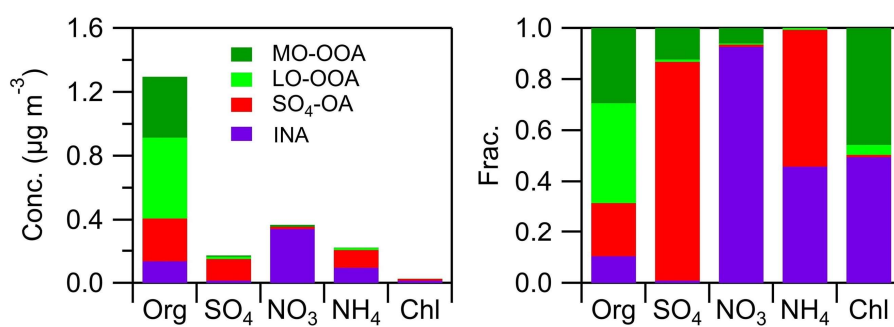


Figure S15. Mass concentrations and mass fractions of NR-PM₁ species in four PMF factors.

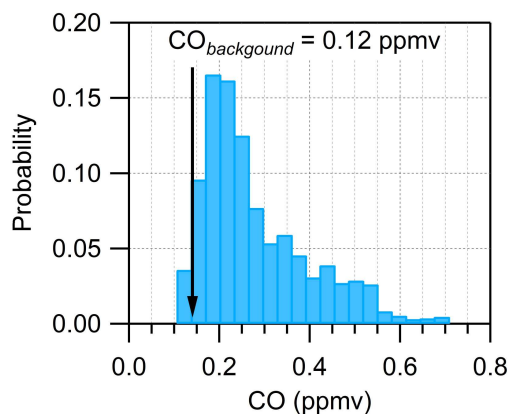


Figure S16. Probability distribution of the mixing ratio of CO during the entire campaign.

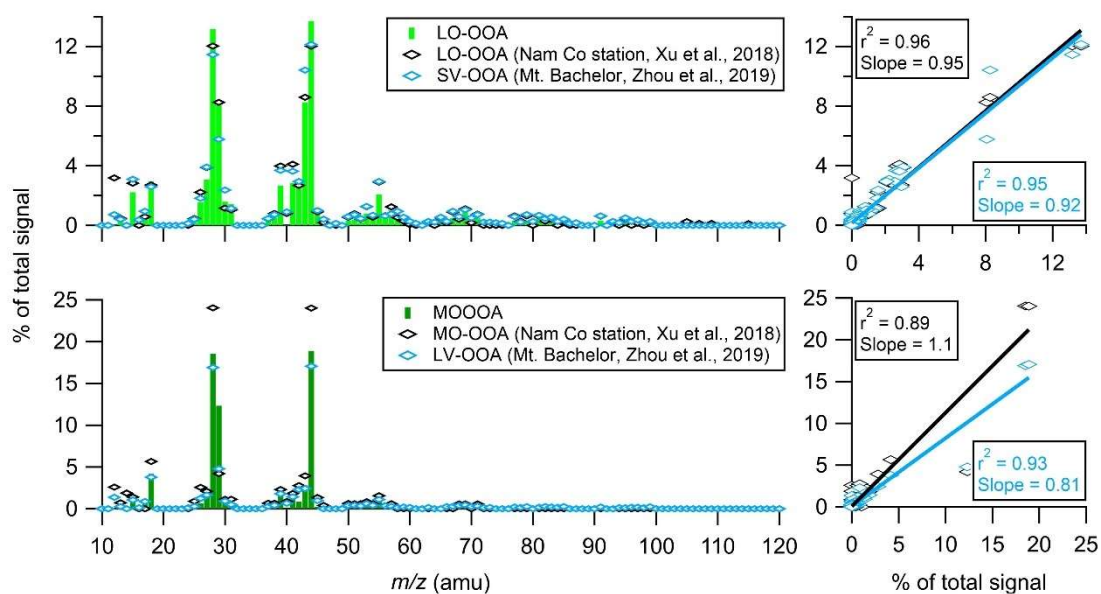


Figure S17. Comparison of the mass spectra of OA in this study with other two mountain stations. The correlation of the mass spectra of these OA factors are also shown.

References

- Du, W., Sun, Y. L., Xu, Y. S., Jiang, Q., Wang, Q. Q., Yang, W., Wang, F., Bai, Z. P., Zhao, X. D., and Yang, Y. C.: Chemical characterization of submicron aerosol and particle growth events at a national background site (3295 m a.s.l.) on the Tibetan Plateau. *Atmos. Chem. Phys.*, 15, 10811-10824, <https://doi.org/10.5194/acp-15-10811-2015>, 2015.
- Petit, J. E., Favez, O., Albinet, A., and Canonaco, F.: A user-friendly tool for comprehensive evaluation of the geographical origins of atmospheric pollution: Wind and trajectory analyses, *Environ. Modell. Softw.*, 88, 183–187, <https://doi.org/10.1016/j.envsoft.2016.11.022>, 2017.
- Paatero, P. and Tapper, U.: Analysis of different modes of factor analysis as least squares fit problems, *Chemometr. Intell. Lab.*, 18, 183–194, 1993.
- Xu, J., Zhang, Q., Shi, J., Ge, X., Xie, C., Wang, J., Kang, S., Zhang, R., and Wang, Y.: Chemical characteristics of submicron particles at the central Tibetan Plateau: insights from aerosol mass spectrometry, *Atmos. Chem. Phys.*, 18, <https://doi.org/10.5194/acp-18-427-2018>, 2018.
- Ulbrich, I. M., Canagaratna, M. R., Zhang, Q., Worsnop, D. R., and Jimenez, J. L.: Interpretation of organic components from Positive Matrix Factorization of aerosol mass spectrometric data, *Atmos. Chem. Phys.*, 9, 2891-2918, <https://doi.org/10.5194/acp-9-2891-2009>, 2009.
- Zhang, Y. M., Zhang, X. Y., Sun, J. Y., Hu, G. Y., Shen, X. J., Wang, Y. Q., Wang, T. T., Wang, D. Z., and Zhao, Y.: Chemical composition and mass size distribution of PM₁ at an elevated site in central east China. *Atmos. Chem. Phys.*, 14, 12237-12249, <https://doi.org/10.5194/acp-14-12237-2014>, 2014.
- Zhu, Q., He, L. Y., Huang, X. F., Cao, L. M., Gong, Z. H., Wang, C., Zhuang, X., and Hu, M.: Atmospheric aerosol compositions and sources at two national background sites in northern and southern China. *Atmos. Chem. Phys.*, 16, 10283-10297, <https://doi.org/10.5194/acp-16-10283-2016>, 2016
- Zhang, X., Xu, J., Kang, S., Zhang, Q., and Sun, J.: Chemical characterization and sources of submicron aerosols in the northeastern Qinghai–Tibet Plateau: insights from high-resolution mass spectrometry. *Atmos. Chem. Phys.* 19, 7897-7911, <https://doi.org/10.5194/acp-19-7897-2019>, 2019.
- Zheng, J., Hu, M., Du, Z., Shang, D., Gong, Z., Qin, Y., Fang, J., Gu, F., Li, M., Peng, J., Li, J., Zhang, Y., Huang, X., He, L., Wu, Y., and Guo, S.: Influence of biomass burning from South Asia at a high-altitude mountain receptor site in China. *Atmos. Chem. Phys.*, 17, 6853-6864, <https://doi.org/10.5194/acp-17-6853-2017>, 2017.
- Zhou, S., Collier, S., Jaffe, D. A., and Zhang, Q.: Free tropospheric aerosols at the Mt. Bachelor Observatory: more oxidized and higher sulfate content compared to boundary layer aerosols, *Atmos. Chem. Phys.*, 19, 1571-1585, <https://doi.org/10.5194/acp-19-1571-2019>, 2019.